A general phase retrieval algorithm based on a ptychographical iterative engine for coherent diffractive imaging*

Fu Jian(傅 健)† and Li Peng(李 鹏)

Research Center of Digital Radiation Imaging and Biomedical Imaging, Beijing University of Aeronautics and Astronautics, Beijing 100191, *China*

(Received 26 April 2012; revised manuscript received 19 July 2012)

Coherent diffractive imaging (CDI) is a lensless imaging technique and can achieve a resolution beyond the Rayleigh or Abbe limit. The ptychographical iterative engine (PIE) is a CDI phase retrieval algorithm that uses multiple diffraction patterns obtained through the scan of a localized illumination on the specimen, which has been demonstrated successfully at optical and X-ray wavelengths. In this paper, a general PIE algorithm (gPIE) is presented and demonstrated with an He–Ne laser light diffraction dataset. This algorithm not only permits the removal of the accurate model of the illumination function in PIE, but also provides improved convergence speed and retrieval quality.

Keywords: phase retrieval algorithm, coherent diffractive imaging, ptychography

PACS: 42.30.Rx, 42.25.Fx **DOI:** 10.1088/1674-1056/22/1/014204

1. Introduction

Coherent diffractive imaging (CDI) relies on far-field diffraction data to retrieve the complex-valued projection or three-dimension density of a specimen.[1] It removes the use of high-quality high-efficiency lenses, and a resolution beyond the Rayleigh or Abbe limit can be achieved. This technique has progressed significantly since its first experimental demonstration in 1999[2] and has been applied to life and material science successfully,[3] such as cells,[4,5] nano-crystals,[6,7] and nano-particles.[8]

A fundamental drawback of CDI is the phase problem: the recorded real-valued data contain only amplitude information, the equally important knowledge of phase values is lost.[9–11] Various solutions have been suggested to retrieve the phase information. Most of them belong to the support-based or ptychography-based approach. The former requires the reconstructed image to be zero-valued outside a given region, corresponding to a finite support bounding the specimen in the physical experiment.[12] It is suitable for CDI of a small and isolated specimen. The latter adopts a scanning mode, called ptychography and was first proposed for electron diffraction in the 1970s,[13,14] to create redundancy in the data by taking diffraction patterns at multiple different but overlapping illumination regions. Then the reconstruction algorithm is applied to the dataset to retrieve the phase information. It permits the reconstruction of non-isolated samples and has attracted much more interest.

For a ptychographical dataset, while an analytic solution via Wigner distribution deconvolution is possible if the step size corresponds to the imaging resolution,[15,16] an iterative algorithm called ptychographical iterative engine (PIE)[17,18] marks a significant improvement. It can robustly retrieve the sample without the common problems in CDI, such as the limited field of view, focal plane ambiguity, non-unique solutions, slow convergence, and so on. The performance of this algorithm has been experimentally demonstrated with laser light and X-rays.[19,20] But a drawback of PIE is the need to accurately model the localized wavefront (the probe) illuminating the target object, which limits PIE's use in situations where it is time-consuming or impossible to measure the probe with good enough accuracy. In recently published papers, this question was addressed by using a difference map algorithm,[21] a non-linear optimization approach,[22] and the extended PIE (ePIE).[23] Here we present an alternative algorithm, a general PIE algorithm (gPIE), which not only permits the removal of the accurate model of the probe, but also provides improved convergence speed and retrieval quality.

2. General PIE algorithm

In order to provide a basis for the following discussion, we briefly introduce the ptychographical scanning mode first. The setup can be as simple as the one shown in Fig. 1. An illumination probe is formed by an aperture close to the plane of the sample or by the focusing of a beam using a lens. This probe, described by complex-valued function $P(\boldsymbol{r}-\boldsymbol{r}_j)$, is incident on the complex-valued object $O(\boldsymbol{r})$. The resulting exit

*Project supported by the National Natural Science Foundation of China (Grant Nos. 11179009 and 50875013), the Beijing Municipal Natural Science Foundation, China (Grant No. 4102036), and the Beijing NOVA Program, China (Grant No. 2009A09).

†Corresponding author. E-mail: fujian706@buaa.edu.cn

© 2013 Chinese Physical Society and IOP Publishing Ltd

wave $\Psi_j(\boldsymbol{r}) = P(\boldsymbol{r}-\boldsymbol{r}_j)O(\boldsymbol{r})$[19] evolves in the far field to a complex-valued diffraction pattern. The detector records this diffraction pattern's intensity $I_j(\boldsymbol{q})$, which is proportional to the squared modulus of the Fourier transform of the exit wave $I_j(\boldsymbol{q}) \propto |F[\Psi_j(\boldsymbol{r})]|^2$. Then the probe or the object is moved relative to each other so that a different region of the object is illuminated strongly in each position and the corresponding diffraction pattern is recorded. This measurement is repeated until the region of interest of the object is covered. In the above complex-valued functions, $\boldsymbol{r}$ and $\boldsymbol{q}$ are real-space and reciprocal-space coordinate vectors, respectively. The vector $\boldsymbol{r}_j$ encodes the relative shift introduced between the object and the probe. The phase retrieval algorithm aims to reconstruct the probe and the object from the measured diffraction patterns.

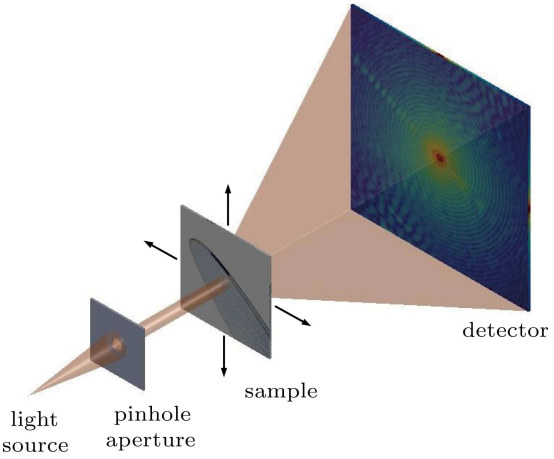


Fig. 1. (color online) Schematic diagram of the experimental setup for ptychographical coherent X-ray diffraction microscopy. The pinhole aperture defines the coherent portion of the incident beam that is used for the experiment. The object can be moved in the plane perpendicular to the propagation direction of the incident beam. The diffraction pattern is recorded with a detector.

Here we introduce the proposed gPIE algorithm, whose implementation steps are described as follows. Initial guesses $O_0(\boldsymbol{r})$ and $P_0(\boldsymbol{r})$ of the object and the probe waveforms are required to begin the algorithm. The iterative number is labeled by n.

(i) The exit wave is calculated from the current guesses of the object and the probe

$$\Psi_{n,j}(\boldsymbol{r}) = P_n(\boldsymbol{r}-\boldsymbol{r}_j)O_n(\boldsymbol{r}). \tag{1}$$

(ii) The modulus of the Fourier transform of this exit wave is replaced with the square root of the corresponding recorded diffraction pattern

$$\Psi_{n,j}(\boldsymbol{q}) = \sqrt{I_j(\boldsymbol{q})}\frac{F[\Psi_{n,j}(\boldsymbol{r})]}{|F[\Psi_{n,j}(\boldsymbol{r})]|}. \tag{2}$$

(iii) An updated exit wave is then obtained via an inverse Fourier transform

$$\Psi'_{n,j}(\boldsymbol{r}) = F^{-1}[\Psi_{n,j}(\boldsymbol{q})]. \tag{3}$$

(iv) The new guess of the object is formed by dividing out the current probe from the updated exit wave and taking a weighted average of this function and the current object guess

$$\begin{aligned} O_{n+1}(\boldsymbol{r}) &= O_n(\boldsymbol{r}) + F_P \times \frac{P_n^*(\boldsymbol{r}-\boldsymbol{r}_j)}{|P_n(\boldsymbol{r}-\boldsymbol{r}_j)|^2+\varepsilon} \\ &\quad \times \left[\Psi'_{n,j}(\boldsymbol{r}) - \Psi_{n,j}(\boldsymbol{r})\right], \end{aligned} \tag{4}$$

where

$$F_P = \left[\frac{|P_n(\boldsymbol{r}-\boldsymbol{r}_j)|}{\max(|P_n(\boldsymbol{r}-\boldsymbol{r}_j)|)}\right]^{\sigma},$$

and ε is a minimum value used to prevent a divide-by-zero occurring.

(v) The new guess of the probe is formed by dividing out the current object from the updated exit wave and taking a weighted average of this function and the current probe guess

$$\begin{aligned} P_{n+1}(\boldsymbol{r}) &= P_n(\boldsymbol{r}) + F_O \times \frac{O_n^*(\boldsymbol{r}+\boldsymbol{r}_j)}{|O_n(\boldsymbol{r}+\boldsymbol{r}_j)|^2+\varepsilon} \\ &\quad \times [\Psi'_{n,j}(\boldsymbol{r}) - \Psi_{n,j}(\boldsymbol{r})], \end{aligned} \tag{5}$$

where

$$F_O = \left[\frac{|O_n(\boldsymbol{r}+\boldsymbol{r}_j)|}{\max(|O_n(\boldsymbol{r}+\boldsymbol{r}_j)|)}\right]^{\sigma}.$$

(vi) Steps (i)–(v) are repeated for each position until the iteration reaches convergence. The convergence is monitored via a normalized sum of the square deviations[23]

$$E = \frac{\sum_{\boldsymbol{q},j}\left|\sqrt{I_j(\boldsymbol{q})} - |F[P_{n+1}(\boldsymbol{r}-\boldsymbol{r}_j)O_{n+1}(\boldsymbol{r})]|\right|^2}{\sum_{\boldsymbol{q},j} I_j(\boldsymbol{q})}. \tag{6}$$

Analyzing this gPIE algorithm, we get the following conclusions:

i) In this algorithm, the accurate model of the probe is no longer known in advance and could be retrieved simultaneously together with the object.

ii) The update functions in steps (iv) and (v) play key roles. The expressions F_P and F_O favor the influence of those areas of the object which have been strongly illuminated, and attenuate the errors which otherwise arise when the illumination is weak.[17] The parameter σ can adjust the amount of this influence and consequently control both the retrieval quality and the convergence. Higher values of σ can magnify the importance of the strongly illuminated area and reduce the contribution of the weakly illuminated area, so they can suppress noise since the weakly illuminated area has a bigger noise than the strongly illuminated area. However, higher values of σ may also lose some details of the retrieved object or probe since the noise and some useful signals may occupy the same frequency range.

iii) The values of F_P and F_O are smaller than 1.0, so higher values of σ will decrease the update step size and slow down the convergence.

The above analyses imply that there exists an optimal value of σ, which can suppress the noise and meanwhile reserve the details. Consequently this algorithm may provide improved convergence speed and retrieval quality by adopting an optimal value of σ.

Comparing this general ptychographical iterative engine with the conventional ptychographical iterative engine, we can find that they are the same when the probe is known and $\sigma = 1.0$. In this case, step (v) can be ignored, and the guess probe in step (iv) will be replaced by the known probe. Furthermore, the recently presented extended ptychographical iterative engine algorithm is also a special case of this general ptychographical iterative engine with $\sigma = 2.0$. In those two algorithms, the values of σ are fixed to be 1.0 and 2.0 respectively. According to the above analyses, they may not provide the best retrieval for the real experimental ptychographical dataset with different noise levels.

3. Simulation

A numerical simulation is executed to investigate the performance of the gPIE algorithm by evaluating the convergence and the reconstruction quality with different values of σ.

Two images, depicted in Figs. 2(a) and 2(b) each with 512×512 pixels, are used as the object phase and modulus profiles, respectively. The modulus image is scaled to values in the range 0.2–1.0 and the phase to values between $\pm\pi$. The object is illuminated in a 11×11 regular grid, and a random offset is added to it to suppress the periodic pattern. The overlap size is set to be 75%. The radius of aperture is 40 pixels, and the pixel size is 5 μm × 5 μm. The probe is generated by propagating this aperture a short distance and is shown in the insets of Figs. 2(a) and 2(b). Far-field diffraction patterns are simulated from this arrangement with the Poisson distributed noise introduced. Figure 2(c) shows one of the diffraction patterns.



(a) (b) (c)

Fig. 2. (color online) An illustration of the object and the probe used to generate the simulated diffraction patterns. (a) Simulated object and probe amplitudes. (b) Simulated object and probe phases. (c) One of simulated patterns (logarithmic scale). The probe is shown in the inserts.

Since the true object wavefront, denoted as $O(\boldsymbol{r})$, is known in the simulated case, the convergence and the reconstruction quality of gPIE algorithm can be measured directly using the normalized root mean square error metric[24]

$$E(n) = \frac{\sum_{\boldsymbol{r}} |O(\boldsymbol{r}) - \gamma O_n(\boldsymbol{r})|^2}{\sum_{\boldsymbol{r}} |O_n(\boldsymbol{r})|^2}, \tag{7}$$

which represents the difference between the retrieved results and the samples. The parameter γ allows for the multiplication of the object by a constant, and for a constant phase offset,

$$\gamma = \frac{\sum_{\boldsymbol{r}} O(\boldsymbol{r}) O_n^*(\boldsymbol{r})}{\sum_{\boldsymbol{r}} |O_n(\boldsymbol{r})|^2}, \tag{8}$$

where $O_n(\boldsymbol{r})$ is the reconstructed object distribution after n iterations. In order to avoid any effects and to neglect unilluminated areas, $E(n)$ is calculated over the center area of the reconstruction that is well covered by a number of overlapping probe positions. The solutions can be obtained when $E(n)$ reaches a stable state. A sub-pixel registration algorithm is used to account for lateral translations of the reconstruction with respect to the original object.[24]

Figure 3 shows the simultaneously retrieved object and probe by gPIE with different values of σ after 50 iterations. The Poisson noise is introduced so that the total count in each pattern is approximately 10^6. It demonstrates the validity of gPIE. Figure 4 shows the progresses of the error metric E over 200 iterations using the simulated data with different noise levels. It demonstrates the effects of σ on the convergence speed and the retrieval quality. For all cases, a lower value of σ leads to a faster convergence of gPIE. Meanwhile, there exists a different optimal value of σ for gPIE to produce the best retrieval at a different noise level. For the cases with the counts of photons 10^4, 10^5, 10^6, and 10^7, the optimal values of σ are 4.0, 2.5, 2.0, and 1.0, respectively. It suggests that gPIE may provide better retrievals by adopting an optimal value of σ according to the noise level of the ptychographical dataset.

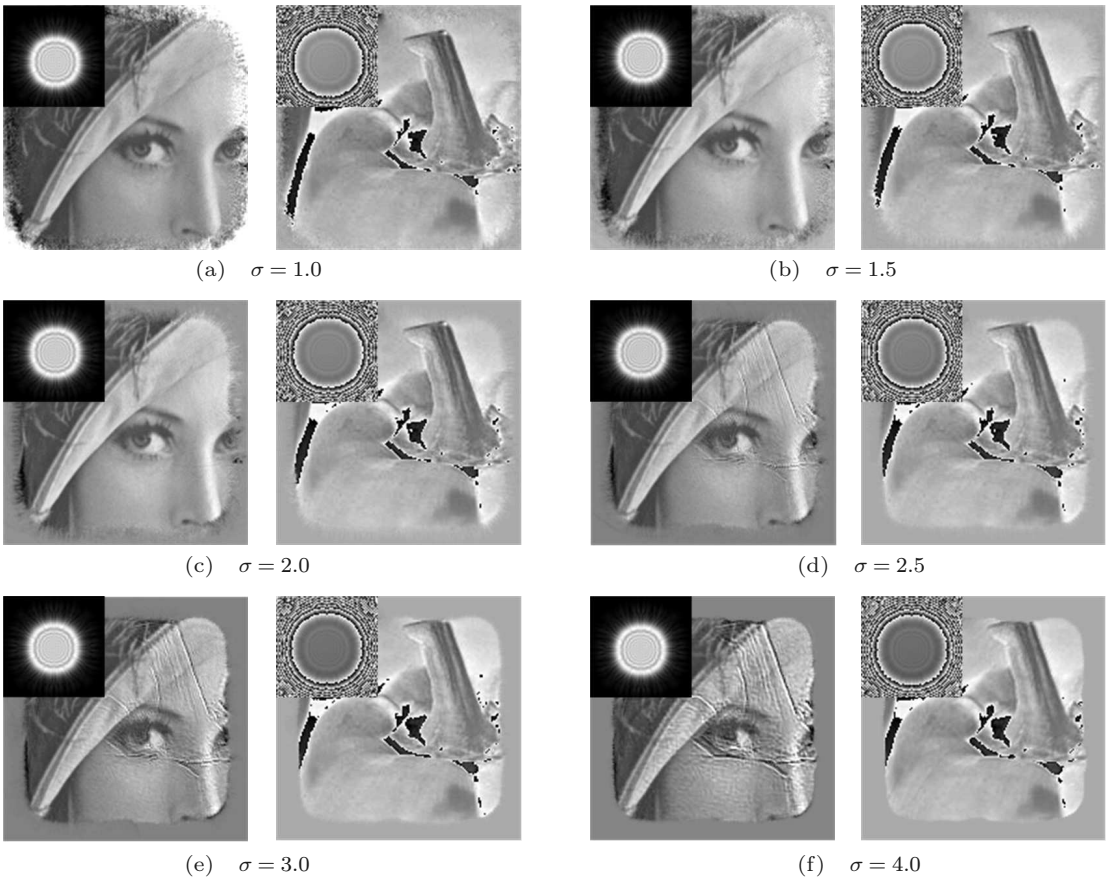


Fig. 3. Reconstructions of gPIE with (a) $\sigma = 1.0$, (b) $\sigma = 1.5$, (c) $\sigma = 2.0$, (d) $\sigma = 2.5$, (e) $\sigma = 3.0$, and (f) $\sigma = 4.0$. The Poisson noise is introduced so that the total count in each pattern is approximately 10^6. In each image, the main figures are the amplitude and phase of the retrieved object respectively, the corresponding insets are the amplitude and phase of the retrieved probe respectively.

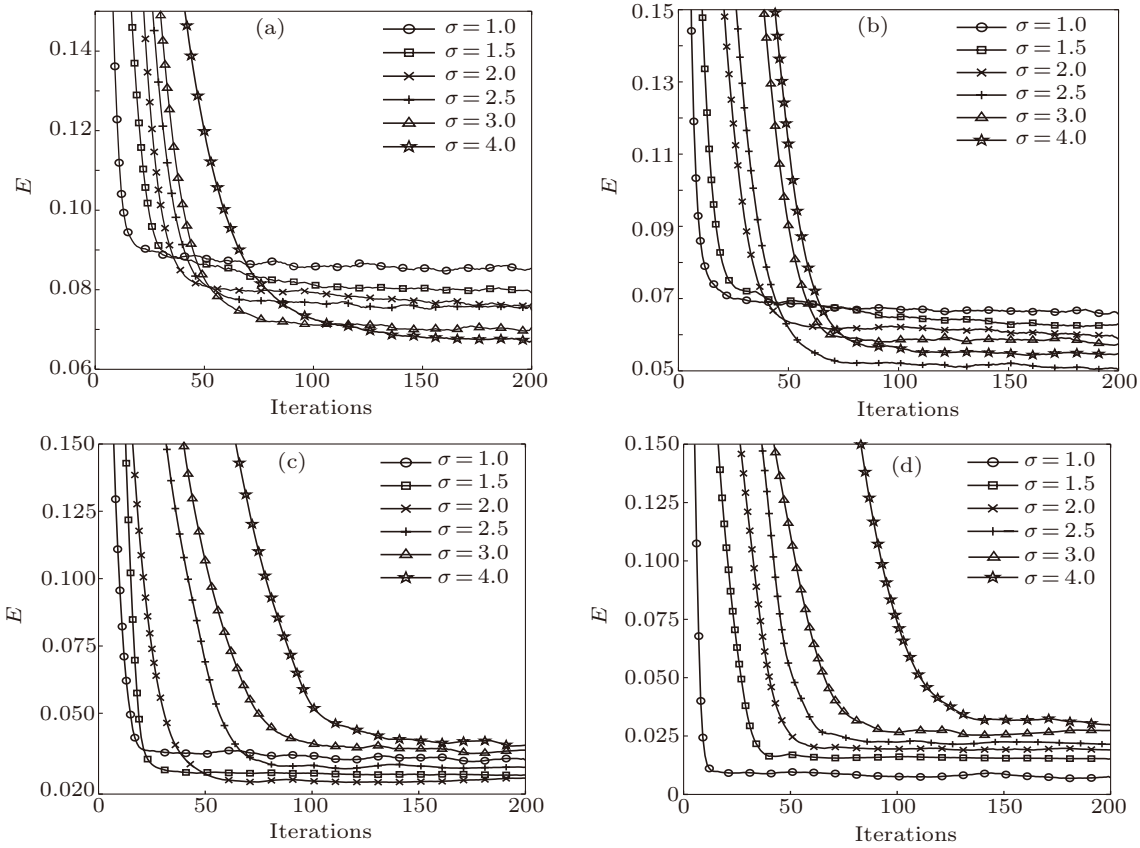


Fig. 4. The progresses of error metric E over 200 iterations using the simulated data with different noise levels. The counts of photons are (a) 10^4, (b) 10^5, (c) 10^6, and (d) 10^7.

4. Optical experiment

An experiment has been conducted in the Paul Scherrer Institut, Villigen, Switzerland to assess the performance of gPIE. The experimental setup is illustrated in Fig. 1. The incident beam was defined by a 200 μm diameter pinhole, which was placed in the path of an He–Ne laser beam, $\lambda = 632.8$ nm. The sample, an insect wing, was mounted on a translation stage and placed about 1 mm behind the pinhole. The detector, a CCD with 24 μm pixel size, was placed at a distance of 140 mm downstream to collect the diffraction patterns. Scattering angles up to 120 mrad in the corners could be collected, leading to a reconstruction pixel size of about 4 μm. During the measurement, the sample was translated to 121 positions in a 11×11 grid with 50 μm step size, corresponding to about 75% probe overlap size.

Since the true object wavefront is no longer available, equation (7) cannot be used as an error measure. Instead, here we use Eq. (6) to measure the normalized error in the diffraction patterns after each full iteration of gPIE.

Using this ptychographical dataset, we firstly investigate the retrieval performance of gPIE with $\sigma = 1.0$, 2.0, 3.0, and 4.0. For each case, the retrieval algorithm runs 200 iterations. The initial guess of the probe is defined as a 200 μm circular aperture. Figure 5 shows the

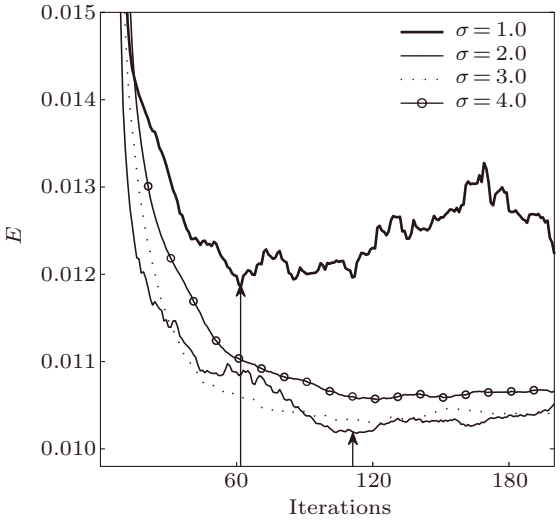


Fig. 5. The progresses of error metric E over 200 iterations of the gPIE with different values of σ. The initial guess of the probe is defined as a 200 μm circular aperture.

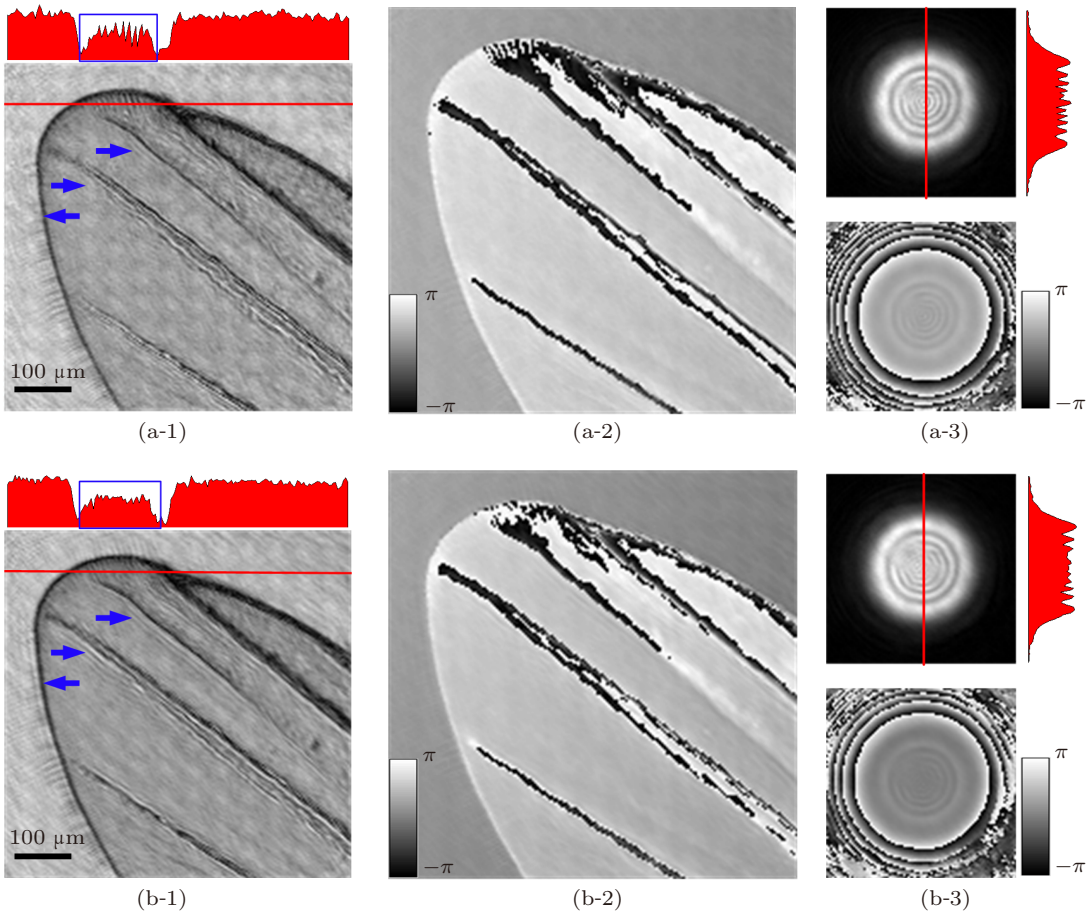


Fig. 6. (color online) Retrievals of gPIE with (a) $\sigma = 1.2$ and (b) $\sigma = 2.0$. Panels (a-1), (b-1) and (a-2), (b-2) are the amplitude and phase parts of the retrieved object, respectively. In panels (a-3) and (b-3), the amplitude and phase parts of the retrieved probe are shown in the top and bottom, respectively. The red profiles along the red horizontal lines in the images indicate that the case with $\sigma = 1.2$ provides much more structural details than that with $\sigma = 2.0$. The blue arrows indicate some regions where the case with $\sigma = 2.0$ produces many more artifacts than that with $\sigma = 1.2$. The red profiles along the red vertical lines in the images demonstrate that the case with $\sigma = 1.2$ retrieves all the fringes of the probe, while the case with $\sigma = 2.0$ produces a probe with some interrupted fringes.

normalized error curves over 200 iterations. It is obvious that different values of σ impose different effects on the retrievals. When $\sigma = 1.0$ and 2.0, the errors reach the minimum after about 60 and 110 iterations, respectively. However, when $\sigma = 3.0$ and 4.0, the errors do not reach the minimum after 200 iterations. It proves that a lower value of σ leads to a faster convergence. Meanwhile, we can also find that a higher value of σ effectively improves the quality of the retrieval. Among these investigated cases, gPIE with $\sigma = 2.0$ provides a better retrieval. However, it may not the best one since only four values of σ are discussed.

In order to get the best retrieval results, we further run gPIE with the values of σ from 1.0 to 3.0 with a step of 0.1. Finally we find that $\sigma = 1.2$ gives the best result. The retrieval results of gPIE with $\sigma = 1.2$ and 2.0 are shown in Fig. 6. Obviously, the red profiles along the red horizontal lines in the the images indicate that the case with $\sigma = 1.2$ provides much more structural details than that with $\sigma = 2.0$. The blue arrows indicate some regions where the case with $\sigma = 2.0$ produces many more artifacts than that with $\sigma = 1.2$. Moreover, the red profiles along the red vertical lines in the images demonstrate that the case with $\sigma = 1.2$ retrieves all the fringes of the probe, while the case with $\sigma = 2.0$ produces a probe with some interrupted fringes. From Fig. 6, we can draw a conclusion that gPIE with $\sigma = 1.2$ provides the best retrieval for this specific ptychographical dataset.

5. Conclusion

In this paper, we have presented a general phase retrieval algorithm based on the ptychographical iterative engine and demonstrated its validity using simulated and experimental data. This algorithm not only permits the removal of the accurate model of the illumination function in PIE and implements the simultaneous retrieval of the probe and the object, but also provides an improved retrieval quality by adjusting the value of the retrieval parameter σ according to the noise level of the ptychographical dataset. Future work will focus on how to quickly determine the optimal value of σ to push its application.

Acknowledgements

We thank Franz Pfeiffer, Martin Dierolf, and Pierre Thibault from the Department of Physics (E17) and Institute of Medical Engineering (IMETUM), Technische Universität München, 85748 Garching, Germany for their fruitful discussion and providing us with the experimental CDI dataset. We also thank Oliver Bunk and Andreas Menzel for their contributions to the experiment at the Paul Scherrer Institute, Villigen, Switzerland.

References

[1] Thibault P, Dierolf M, Bunk O, Menzel A and Pfeiffer F 2009 *Ultramicroscopy* **109** 338
[2] Miao J, Charalambous P, Kirz J and Sayre D 1999 *Nature* **400** 342
[3] Dierolf M, Thibault P, Menzel A, Kewish C M, Jefimovs K, Schlichting I, von König K, Bunk O and Pfeiffer F 2010 *New J. Phys.* **12** 035017
[4] Miao J, Hodgson K, Ishikawa T, Larabell C, LeGros M and Nishino Y 2003 *Proc. Natl. Acad. Sci. USA* **100** 110
[5] Shapiro D, Thibault P, Beetz T, Elser V, Howells M R, Jacobsen C, Kirz J, Lima E, Miao H, Nieman A M and Sayre D 2005 *Proc. Natl. Acad. Sci. USA* **102** 15343
[6] Robinson I, Vartanyants I, Williams G, Pfeifer M and Pitney J 2001 *Phys. Rev. Lett.* **87** 195505
[7] Pfeifer M, Williams G, Vartanyants I, Harder R and Robinson I 2006 *Nature* **442** 63
[8] Chapman H N, Barty A, Marchesini S, Noy A, Cui C, Howells M R, Rosen R, He H, Spence J C H, Weierstall U, Beetz T, Jacobsen C and Shapiro D 2006 *J. Opt. Soc. Am.* A **23** 1179
[9] Bunk O, Dierolf M, Kynde S, Johnson I, Marti O and Pfeiffer F 2008 *Ultramicroscopy* **108** 481
[10] Zhu H F, Xie H L, Gao H Y, Chen J W, Li R X and Xu Z Z 2005 *Chin. Phys.* **14** 796
[11] Liu X, Guo J C and Niu H B 2010 *Chin. Phys.* B **19** 070701
[12] Fienup J R 1982 *Appl. Opt.* **21** 2758
[13] Hegerl R and Hoppe W 1970 *Ber. Bunsenges. Phys. Chem.* **74** 1148
[14] Hoppe W 1969 *Acta Cryst.* A **25** 495
[15] Rodenburg J M and Bates R H T 1992 *Phil. Trans. R. Soc.* A **339** 521
[16] Chapman H N 1996 *Ultramicroscopy* **66** 153
[17] Rodenburg J M and Faulkner H M L 2004 *Appl. Phys. Lett.* **85** 4795
[18] Faulkner H M L and Rodenburg J M 2004 *Phys. Rev. Lett.* **93** 023903
[19] Rodenburg J M, Hurst A C and Cullis A G 2006 *Ultramicroscopy* **107** 227
[20] Rodenburg J M, Hurst A C, Cullis A G, Dobson B R, Pfeiffer F, Bunk O, David C, Jefimovs K and Johnson I 2007 *Phys. Rev. Lett.* **98** 034801
[21] Thibault P, Dierolf M, Menzel A, Bunk O, David C and Pfeiffer F 2008 *Science* **321** 379
[22] Guizar-Sicairos M and Fienup J R 2008 *Opt. Express* **16** 7264
[23] Maiden A M and Rodenburg J M 2009 *Ultramicroscopy* **109** 1256
[24] Guizar-Sicairos M, Thurman S T and Fienup J R 2008 *Opt. Lett.* **33** 156